Self-Oriented Regular Arrays of Carbon Nanotubes and Their Field Emission Properties

Shoushan Fan, Michael G. Chapline, Nathan R. Franklin, Thomas W. Tombler, Alan M. Cassell, Hongjie Dai*

The synthesis of massive arrays of monodispersed carbon nanotubes that are self-oriented on patterned porous silicon and plain silicon substrates is reported. The approach involves chemical vapor deposition, catalytic particle size control by substrate design, nanotube positioning by patterning, and nanotube self-assembly for orientation. The mechanisms of nanotube growth and self-orientation are elucidated. The well-ordered nanotubes can be used as electron field emission arrays. Scaling up of the synthesis process should be entirely compatible with the existing semiconductor processes, and should allow the development of nanotube devices integrated into silicon technology.

Growing organized carbon nanotubes on large-scale surfaces is important for obtaining scaled-up functional devices for use as scanning probes and sensors (*1–5*), as field emitters (*6–11*), and in nanoelectronics (*12*). In this context, it is desirable to be able to grow high-quality nanotubes in a controlled fashion so that little or no post-growth manipulation or assembly is needed to build useful structures. Aligned nanotubes were obtained previously by using chemical vapor deposition (CVD) over catalysts embedded in mesoporous silica (*13, 14*), and over laser-patterned catalysts (*15, 16*). Recently, Ren *et al.* used plasma-enhanced CVD and synthesized self-aligned nanotubes on glass substrates, although the growth and alignment mechanism remained unclear (*17*).

This work develops the synthesis and understanding of well-aligned nanotubes with uniform diameters on silicon substrates. In particular, we find that porous silicon, a light-emitting material (*18, 19*), is an ideal substrate for growing organized nanotubes (Fig. 1). Porous silicon samples were obtained by electrochemical etching of P-doped n^+-type Si(100) wafers (diameter 2 inches, resistivity 0.008 to 0.018 ohm·cm). Etching was carried out in a Teflon cell using a Pt cathode for 5 min under backside illumination with a halogen lamp. The etching solution contained one part hydrogen fluoride (50% aqueous solution) and one part ethanol, and the anodization current density was kept constant at 10 mA/cm^2. The resulting porous silicon has a thin nanoporous layer (with pore diameters of ~3 nm) on top of a macroporous layer (with submicrometer pores) (*20, 21*). Plain silicon substrates were purchased and used as is, without cleaning or removing the native oxide layer. All substrates were patterned with Fe films (5 nm thick) by electron beam evaporation through shadow masks, containing squared openings with side lengths of 10 to 250 μm at pitch distances of 50 to 200 μm. The substrates were then annealed in air at 300°C overnight. This annealing step oxidizes the surface of the silicon and the iron. In the case of porous silicon, the resulting thin oxide layer protects its porous structure from collapsing later in the high-temperature CVD process (*20*). The substrate was placed in a cylindrical quartz boat sealed at one end and then inserted into the center of a 2-inch quartz tube reactor housed in a tube furnace. The furnace was heated to 700°C in flowing Ar. Ethylene was then flown at 1000 sccm for 15 to 60 min, after which the furnace was cooled to room temperature.

Using a scanning electron microscope (SEM), we observed that three-dimensional regular arrays of nanotube blocks or towers were formed on top of the patterned iron squares on the substrates (Fig. 2, A to F). Each nanotube block exhibits very sharp edges and corners in low-magnification SEM images, and no nanotubes are observed branching away from the blocks (Fig. 2, A to E). The width of the blocks is the same as that of the iron patterns. For CVD reaction times of 5 to 60 min, the height of the blocks is in the range of 30 to 240 μm. High-resolution SEM images (Fig. 2F) show that the nanotubes within each block are well aligned along the direction perpendicular to the surface. As the aspect ratio of the blocks approaches ~5, we observe that some blocks become tilted but do not fall down onto the surface.

Transmission electron microscopy (TEM) was used to further characterize the synthesized nanotubes. We used tweezers to pick up several 250 μm by 250 μm nanotube blocks, ultrasonicated them in 1,2-dichloroethane for 15 min, and then placed a few drops of the suspension onto a TEM grid. TEM investigation showed that the material consisted of multiwalled nanotubes (Fig. 2G). The ultrasonicated material still exhibited many aligned multiwalled bundles and some separated individual nanotubes (Fig. 2G). This clearly indicates that the nanotubes within each block are densely packed and held together by van der Waals interactions. Measurements on more than 100 nanotubes showed that ~90% of our multiwalled nanotubes have diameters of 16 ± 2 nm. Relative to previous CVD-grown aligned nanotubes, our nanotubes are straighter, have smaller diameters, and have a narrower diameter distribution (*13–17*). High-resolution TEM images show that our nanotubes contain a low defect density in some sections of their lengths.

Previously, aligned nanotubes were obtained as a result of confining CVD nanotube growth in the pores of mesoporous silica or channels of alumina membranes (*13, 14, 22, 23*) or by means of gravitational effects (*15, 16*). In our growth process, nanotubes self-assemble into aligned structures similar to the recent result of Ren *et al.* (*17*). We have elucidated the growth and alignment mechanism in the current work. First, we were able to confirm that the base-growth mode (*24–27*) dominates in our system. That is, catalyst particles interact strongly with the substrate and remain pinned during growth. Our evidence is that after physically removing nanotube blocks on several samples and heating the substrates in air to 700°C, the resulted substrates were still catalytically active for growing oriented nanotube arrays. This result leads to the self-oriented nanotube growth mechanism (Fig. 3). During the initial stage

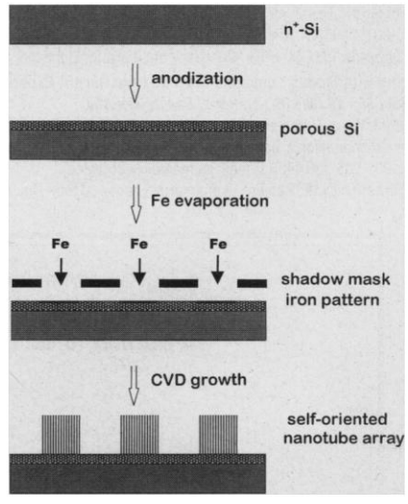

Fig. 1. Schematic process flow for the synthesis of regular arrays of oriented nanotubes on porous silicon by catalyst patterning and CVD.

Department of Chemistry, Stanford University, Stanford, CA 94305, USA.

*To whom correspondence should be addressed. E-mail: hdai@chem.stanford.edu

of CVD, ethylene molecules are catalytically decomposed on the iron oxide nanoparticles. As supersaturation occurs, a nanotube grows off each of the densely packed catalyst particles (average diameter 16 nm) and extends to open space along the direction normal to the substrate. As the nanotubes lengthen, their outermost walls interact with those of neighboring nanotubes via van der Waals forces to form a large bundle with sufficient rigidity. This rigidity enables nanotubes to keep growing along the original direction. Even the outermost nanotubes are held by the inner nanotubes without branching away.

Porous silicon substrates exhibit important advantages over silicon substrates for synthesizing self-oriented nanotubes. Growth on substrates that contained both porous silicon and plain silicon portions showed that the nanotubes grow at a higher rate (length per minute) on porous silicon than on silicon (*28*). This can be attributed to ethylene molecules permeating the porous silicon structures (surface area ~300 m^2/g) (*20*), which feed the nanotube growth more efficiently (Fig. 3). Also, the nanoporous silicon layer acts as an excellent catalyst support. During the 300°C annealing step, iron oxide nanoparticles form with a narrow size distribution because of their strong interactions with the highly porous support. These strong interactions also prevent catalyst particles from sintering at elevated temperatures.

The length of our nanotubes can be controlled by tuning the CVD reaction time. On n^+-type porous silicon substrates with 38 μm by 38 μm patterned catalyst, for reaction times of 5, 15, 30, and 60 min, we grew nanotubes with lengths of ~35, 100, 160, and 240 μm, respectively (*29*).

Carbon nanotubes have been identified as promising candidates for field emitters in applications such as flat panel displays (*6–11*).

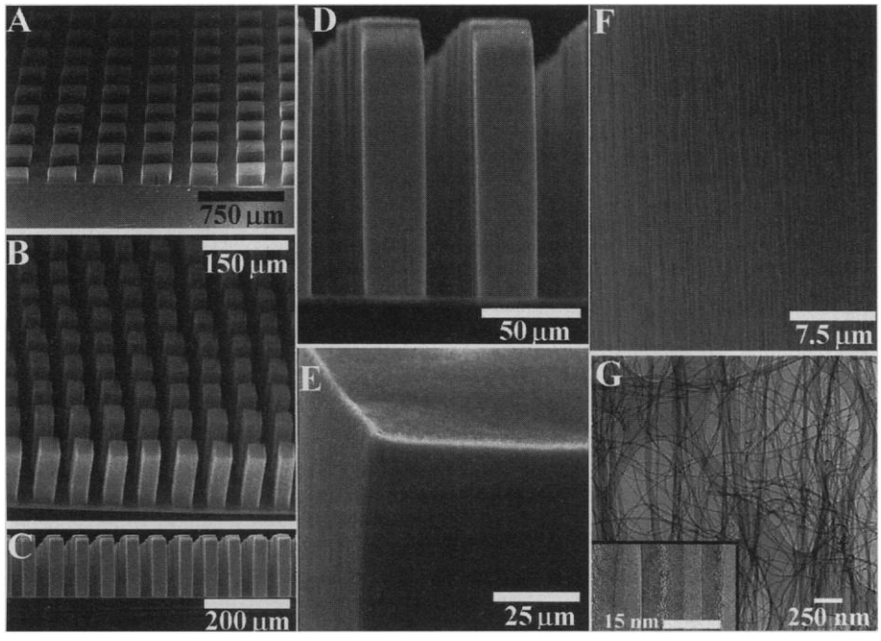

Fig. 2. Electron micrographs of self-oriented nanotubes synthesized on n^+-type porous silicon substrates. (**A**) SEM image of nanotube blocks synthesized on 250 μm by 250 μm catalyst patterns. The nanotubes are 80 μm long and oriented perpendicular to the substrate [see (F)]. (**B**) SEM image of nanotube towers synthesized on 38 μm by 38 μm catalyst patterns. The nanotubes are 130 μm long. (**C**) Side view of the nanotube towers in (B). The nanotubes self-assemble such that the edges of the towers are perfectly perpendicular to the substrate. (**D**) Nanotube "twin towers," a zoom-in view of Fig. 2C. (**E**) SEM image showing sharp edges and corners at the top of a nanotube tower. (**F**) SEM image showing that nanotubes in a block are well aligned to the direction perpendicular to the substrate surface. (**G**) TEM image of pure multiwalled nanotubes in several nanotube blocks grown on a n^+-type porous silicon substrate. Even after ultrasonication for 15 min in 1,2-dichloroethane, the aligned and bundled configuration of the nanotubes is still evident. The inset is a high-resolution TEM image that shows two nanotubes bundling together. The well-ordered graphitic lattice fringes of both nanotubes are resolved.

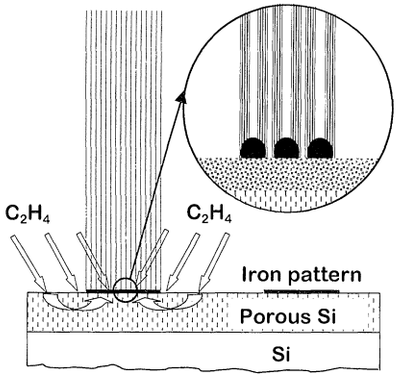

Fig. 3. Nanotube growth and self-orientation on porous silicon substrate. On the substrate, the iron oxide nanoparticles remain pinned down during CVD growth, and thus base growth operates. The ethylene gas molecules feed the growing nanotubes at the edge of the catalyst square by diffusing through the nanotubes and through the porous silicon layer. On a plain silicon substrate, the ethylene molecules can only feed the edge of the catalyst square and diffuse through the nanotubes, which results in a growth rate lower than would be observed on a porous silicon substrate (*28*). The nanotubes within each block interact via van der Waals forces, which provide the overall rigidity for oriented growth. Some openings exist between bundled nanotubes, allowing gas to diffuse.

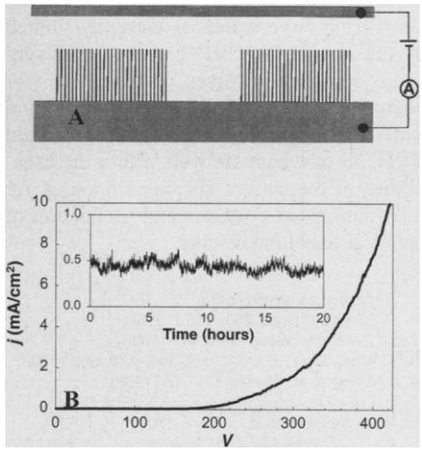

Fig. 4. Self-oriented nanotube arrays as electron field emitter arrays. (**A**) Experimental setup. The cathode consists of a n^+-type porous silicon substrate with four 250 μm by 250 μm nanotube blocks. The height of the blocks is 130 μm. An aluminum-coated silicon substrate serves as the anode and is kept 200 μm away from the sample by a mica spacer containing a hole in the center. (**B**) Current density (j) versus voltage (V) characteristics of the sample. The data were taken in a vacuum chamber at 3×10^{-7} torr and were highly reproducible over repeated voltage scans. Fitting j-V according to the Fowler-Nordheim equation showed two linear regimes joined together, forming a knee, similar to the observation by Collins and Zettl (*7*). The inset shows the emission current stability over a test period of 20 hours at a current density of ~0.5 mA/cm^2. The emission current fluctuates but does not exhibit degradation. After continuous stability test for >100 hours, SEM images show no obvious damage to the nanotube blocks. With ~15 samples, we find that to reach current densities of 1 mA/cm^2 and 10 mA/cm^2, the electric fields (calculated by using the distance from the anode to the top of nanotube blocks) required are 2.7 to 3.3 and 4.8 to 6.1 V/μm (the corresponding electric fields are ~3 and ~5 V/μm with arc-discharge samples) (*6–11*), respectively. The emission current is found to scale linearly with the number of nanotube blocks on the samples.

However, it remains unclear how to scale up these novel devices because of the lack of strategies in scaling up nanotube growth and large-scale nanotube assembly and patterning (*1, 30*). Using the synthesized self-oriented nanotube arrays without further sample processing, we have studied their properties as electron field emission arrays. About 15 samples have been tested, and they all exhibit low operating voltages and high current stability (Fig. 4). Their performances are comparable to the best field emission samples previously constructed by processing arc-discharge multiwalled or single-walled nanotubes (*6, 8–11*). Notably, our approach to these useful devices is via direct chemical synthesis of massive arrays of oriented nanotubes on macroscopic substrates.

We have synthesized regular arrays of oriented nanotubes with high uniformity on substrates with typical size ~2 cm by 2 cm. Growth on large wafers is currently limited by the size of the CVD chamber. Our synthetic approach involves porous silicon or plain silicon substrates, metal evaporation and annealing for catalyst formation, and CVD, all of which are well within the capabilities of the current silicon technology for fully automated synthesis and production of practical nanotube devices.

References and Notes

1. R. Service, *Science* **281**, 940 (1998).
2. H. Dai *et al.*, *Nature* **384**, 147 (1996).
3. S. Wong *et al.*, *J. Am. Chem. Soc.* **120**, 603 (1998).
4. S. Wong *et al.*, *Nature* **394**, 52 (1998).
5. H. Dai *et al.*, *Appl. Phys. Lett.* **73**, 1508 (1998).
6. W. A. de Heer *et al.*, *Science* **270**, 1179 (1995).
7. P. G. Collins and A. Zettl, *Appl. Phys. Lett.* **69**, 1969 (1996).
8. Q. Wang *et al.*, *ibid.* **72**, 2912 (1998).
9. Q. H. Wang *et al.*, *ibid.* **70**, 3308 (1997).
10. J.-M. Bonard *et al.*, *ibid.* **73**, 918 (1998).
11. Y. Saito *et al.*, *Ultramicroscopy* **73**, 1 (1998).
12. S. Tans *et al.*, *Nature* **393**, 49 (1998).
13. W. Li *et al.*, *Science* **274**, 1701 (1996).
14. Z. Pan *et al.*, *Nature* **394**, 631 (1998).
15. M. Terrones *et al.*, *ibid.* **388**, 52 (1997).
16. M. Terrones *et al.*, *Chem. Phys. Lett.* **285**, 299 (1998).
17. Z. F. Ren *et al.*, *Science* **282**, 1105 (1998).
18. L. T. Canham, *Appl. Phys. Lett.* **57**, 1046 (1990).
19. R. T. Collins *et al.*, *Phys. Today* **50**, 24 (1997).
20. J.-C. Vial and J. Derrien, Eds., *Porous Silicon Science and Technology: Winter School, Les Houches, 1994* (Springer-Verlag, Berlin, 1994).
21. R. L. Smith and S. D. Collins, *J. Appl. Phys.* **71**, R1 (1992).
22. G. Che *et al*, *Nature* **393**, 346 (1998).
23. T. Kyotani *et al.*, *Chem. Mater.* **8**, 2109 (1996).
24. S. Amelinckx *et al.*, *Science* **265**, 635 (1994).
25. R. T. K. Baker, *Carbon* **27**, 315 (1989).
26. G. G. Tibbetts, *J Cryst. Growth* **66**, 632 (1984).
27. J. Kong *et al.*, *Chem. Phys. Lett.* **292**, 567 (1998).
28. We have grown regular arrays of oriented nanotube blocks on plain Si(100) substrates (we typically use B-doped p-type wafers, resistivity 5 to 10 ohm·cm). The overall structures of the nanotube blocks are similar to those grown on porous silicon. However, in contrast to porous silicon, we often find many nanotube towers with aspect ratio ≥5 falling onto the surface. This indicates weaker interactions at the interfaces between the nanotubes and the flat silicon surface. Also, the nanotubes appear to be less well aligned on plain silicon substrates than on the porous silicon. TEM studies show that the nanotubes synthesized on plain silicon substrates have larger diameters and broader diameter distributions than those on porous silicon.
29. The growth rate seems to be linear initially and tends to level off at longer time reactions (S. Fan, M. Chapline, N. Franklin, H. Dai, unpublished data).
30. D. Normile, *Science* **281**, 632 (1998).
31. S.F. is on leave from the Department of Physics, Tsinghua University, Beijing, China.

We thank C. Quate and H. Soh for helpful discussions. Supported by NSF, a Camille and Henry Dreyfus New Faculty Award, the American Chemical Society–Petroleum Research Fund, and the Center for Materials Research at Stanford University.

13 October 1998; accepted 4 December 1998

Pulmonary Function and Metabolic Physiology of Theropod Dinosaurs

John A. Ruben,* Cristiano Dal Sasso,† Nicholas R. Geist,† Willem J. Hillenius,† Terry D. Jones,† Marco Signore†

Ultraviolet light analysis of a fossil of the theropod dinosaur *Scipionyx samniticus* revealed that the liver subdivided the visceral cavity into distinct anterior pleuropericardial and posterior abdominal regions. In addition, *Scipionyx* apparently had diaphragmatic musculature and a dorsally attached posterior colon. These features provide evidence that diaphragm-assisted lung ventilation was present in theropods and that these dinosaurs may have used a pattern of exercise physiology unlike that in any group of living tetrapods.

Lung structure and ventilation in theropod dinosaurs is assumed to have resembled the specialized flow-through, air sac pulmonary system of extant birds, the closest living relatives of the theropods (*1*). However, some fossil soft tissue evidence, as well as osteological similarities between crocodilians and theropods, suggests that these dinosaurs may have had relatively unmodified septate lungs that were ventilated with the assistance of an active, hepatic piston–diaphragm mechanism (*2*). Those conclusions are based, in part, on the distinct, vertically oriented, thoracic-abdominal separation of the visceral cavity in the theropod *Sinosauropteryx* (Coelurosauria: Compsognathidae) (Fig. 1, bottom). Additionally, the leading edge of the abdominal cavity in this dinosaur appears to have been defined by a remarkably crocodilian-like, anterior surface of the liver. These attributes, as well as the ubiquitous occurrence among theropods of a triradiate pelvis similar to that of crocodilians, well-developed gastralia, and specialized rib morphology (*3*), suggest that these dinosaurs had a crocodilian-like septate lung that was ventilated, in part, with a hepatic piston diaphragm. Such a diaphragm was likely to have been powered by diaphragmatic muscles that extended between the pubes, gastralia, and liver (*2*).

A recently described new theropod from Italy, *Scipionyx samniticus* (Coelurosauria: Maniraptoriformes), contains nearly complete preservation of the articulated skeleton (*4*). The specimen also has remnants of a variety of soft tissues, including portions of the intestines, liver, trachea, and skeletal muscles (Fig. 1, top). Here we describe these soft tissues and discuss their implications for pulmonary structure and function in *Scipionyx*. We also discuss their significance for earlier conclusions about theropod lung morphology and function.

Portions of the large intestine and trachea of *Scipionyx* are visible and appear to have been preserved in situ (Fig. 1) (*4, 5*). Notably, the posterior colon, or colorectal intestine, is situated far dorsally, at about the same level as the vertebrae in the lumbar-sacral region. This condition is comparable to the position of the colon in living taxa such as crocodilians and mammals (Fig. 2A) (*6*). In contrast, the colon (or rectum) of birds is invariably suspended by the dorsal mesentery (mesocolon) so that it is situated in the mid-abdominal cavity, some distance from the roof of the cavity (Fig. 2B) (*7*). This mid-abdominal suspension of avian large (and small) intestines provides a distinct segregation of the colon from the dorsally and medially attached abdominal air sacs (which extend caudally from the dorsally attached parabronchi). Therefore, it is unlikely that avian-style, abdominal air sacs were present in *Scipionyx*. Abdominal air sacs are of fundamental importance to the function of both neo- and paleopulmo por-

J. A. Ruben, N. R. Geist, T. D. Jones, Zoology Department, Oregon State University, Corvallis, Oregon 97331, USA. C. Dal Sasso, Museo Civico di Storia Naturale, Corso Venezia 55, Milano 20121, Italy. W. J. Hillenius, Department of Biology, College of Charleston, Charleston, SC 29424, USA. M. Signore, Department of Geology, University of Bristol, Bristol BS8 1RJ, UK.

*To whom correspondence should be addressed.
†Secondary authors are listed alphabetically.